

Simple El Niño prediction scheme using the signature of climate time series

Nozomi Sugiura^a, Shinya Kouketsu^a

^aResearch Institute for Global Change, Japan Agency for Marine-Earth Science and Technology, Yokosuka, Japan

ARTICLE INFO

Keywords:
signature
El Niño
time series analysis
machine learning

ABSTRACT

El Niño is a typical example of a coupled atmosphere–ocean phenomenon, but it is unclear whether it can be described quantitatively by a correlation between relevant climate events. To provide clarity on this issue, we developed a machine learning-based El Niño prediction model that uses the time series of climate indices. By transforming the multidimensional time series into the path signature, the model is able to properly evaluate the order and nonlinearity of climate events, which allowed us to achieve good forecasting skill (mean square error = 0.596 for 6-month prediction). In addition, it is possible to provide information about the sequence of climate events that tend to change the future NINO3.4 sea surface temperatures. In forecasting experiments conducted, changes in the North Pacific Index and several NINO indices were found to be important precursors. The results suggest that El Niño is predictable to some extent based on the correlation of climate events.

CRediT authorship contribution statement

Nozomi Sugiura: Conceptualization, Methodology, Software, Writing- Original draft preparation.. **Shinya Kouketsu:** Investigation, Writing- Reviewing and Editing..

1. Introduction

El Niño is an important climate phenomenon that has an immense socio-economic impact. Consequently, its onset/offset mechanism has been garnering intense scientific interest (Neelin et al., 1998; Wallace et al., 1998; Timmermann et al., 2018), and the relationships with the other climate modes and events has been investigated (Bjerknes, 1969; Alexander et al., 2002; White et al., 2014) for many years. The prediction of El Niño events is still under investigation from various perspectives, including statistical inference from past time series of climate records and results from climate models, initialization from climate models, and data assimilation using oceanic or coupled atmospheric–oceanic models.

Although previous studies suggest that predictions with expensive climate models outperform purely statistical predictions (Wu et al., 2021), statistical predictions still appear to have value because of their simplicity (Penland and Magorian, 1993). Recently, elaborate and quite skillful predictions have been performed based on machine learning, or deep learning, with the use of past oceanic sea surface temperatures (SSTs) and subsurface information (Wang et al., 2020; Ham et al., 2019). Hu et al. (2021) extensively evaluated the climate network method that utilizes the relationship between spatio-temporal points and concluded that it has some prediction skill over one year. Dijkstra et al. (2019) also reported that machine learning models can improve the prediction skill over one year. Nonetheless, few practical

ORCID(s): 0000-0001-6634-1340 (N. Sugiura)

prediction studies have employed only the series of multidimensional climate indices as learning datasets. As a remarkable exception, Yan et al. (2020) used the NINO3.4 and Southern Oscillation indices exclusively and successfully performed a skillful prediction of the NINO3.4 index via a temporal convolutional network. In light of the well-known fact that the climate events and variabilities in the extratropics can also modulate El Niño and the Southern Oscillation (ENSO) variability (Vimont et al., 2003; Nakamura et al., 2006), the use of the various climate indices, which represent the typical patterns of the ocean surface variables (e.g., sea surface temperature and sea level pressure) in the course of climate changes, can simply clarify the relationships between ENSO and the other climate modes as well as improve the prediction efficiency of ENSO. However, a possible disadvantage of statistical predictions is that they typically provide little information about the correlations among these climate events through their evolution.

To rectify this issue, we propose a new statistical method that is simple, considerably skillful, and provides process information to explain how climate events evolved. This study was conducted to develop a practical machine learning-based El Niño prediction scheme using the past time series of climate indices. The key ingredient that enables the faithful interpretation of the past time series, including their nonlinearities, is the signature of paths, which is a central concept in rough path theory (Lyons et al., 2007).

Although several studies have been published on the methodology of time series analysis using the signature method (Morrill et al., 2021), there appears to be no application of the method to global-scale climate events, and thus this paper opens a new field of research in geosciences.

2. Methodology

In this study, we apply supervised learning to a time series of past climate indices. We utilize the fact that each segment of the time series is an explanatory variable that is equipped with future values at that time, which can be regarded as objective variables. The most significant aspect of the proposed method is that each segment of the time series is transformed into a signature. Therefore, our case study simply employs the simplest setting, utilizing the signature method to concentrate on the proof-of-concept. In this section, after explaining the theoretical basis of why the signatures are relevant, we present the machine learning procedure based on that theory. Then, we discuss how to interpret the results and, finally, we present the parameters used.

2.1. Approximating a function on a set of paths

In prediction study based on the learning of time series, it is crucial to properly construct a predictor that link past time series segments to future values. A predictor is represented as a continuous function on a set of multidimensional paths. To secure the performance of the predictor, it is essential to choose an appropriate basis for the function of the path because it determines the expressive power of the function. Note that our concern is not the basis for a path

but for a function of paths. In this sense, the most mathematically justified candidate for the basis is the signature (Lyons et al., 2007; Sugiura and Hosoda, 2020).

For a d -dimensional path $X = X_{[s,t]} : [s, t] \rightarrow \mathbb{R}^d$ that maps τ to X_τ , the 0-th to n -th iterated integrals are defined recursively, as follows (Lyons et al., 2007):

$$S^0(X_{[s,t]}) = 1, \tag{1}$$

$$S^{(i_1 \dots i_n)}(X_{[s,t]}) = \int_s^t S^{(i_1 \dots i_{n-1})}(X_{[s,t_n]}) dX_{t_n}^{(i_n)}, \quad i_1, \dots, i_n = 1, \dots, d. \tag{2}$$

The signature $S(X)$ of path X is the collection of all the iterated integrals, and the operation $S : X \mapsto S(X)$ is called the signature transform. In particular, its truncation up to the n -th iterated integrals is called the step- n signature, $S_n(X) \in \bigoplus_{k=0}^n (\mathbb{R}^d)^{\otimes k}$, which means that the multi-index I in component $S_n^{(I)}(X_{[s,t]})$ runs across

$$I \in \phi \cup \{1, \dots, d\} \cup \dots \cup \{1, \dots, d\}^n. \tag{3}$$

Now, let $C(K, \mathbb{R})$ be the space of a continuous function on a compact set K of paths with at least one monotonous coordinate. Subset $A \subset C(K, \mathbb{R})$ is defined as

$$A = \left\{ g : X \mapsto \sum_I w^{(I)} S^{(I)}(X) \mid w \in \bigoplus_{k=0}^n (\mathbb{R}^d)^{\otimes k} \text{ for some } n \geq 0 \right\}. \tag{4}$$

Then, A satisfies the following conditions:

1. Because the step- n signature transform $K \ni X \mapsto S_n(X)$ is continuous for any $n > 0$, $A \subset C(K, \mathbb{R})$.
2. $g_1, g_2 \in A$ and $\lambda_1, \lambda_2 \in \mathbb{R} \implies \lambda_1 g_1 + \lambda_2 g_2 \in A$.
3. Constant-valued function $\mathbf{1} \in A$.
4. Based on the shuffle identity (Lyons et al., 2007), $g_1, g_2 \in A \implies g_1 g_2 \in A$.
5. Based on the uniqueness theorem (Levin et al., 2013), for all $X, Y \in A$ with $X \neq Y$, there exists $g \in A$ that satisfies $g(X) \neq g(Y)$.

From these conditions, we can apply the Stone–Weierstrass theorem (Stone, 1937) to the subset A and conclude that A is dense in $C(K, \mathbb{R})$, which means that any function $f \in C(K, \mathbb{R})$ is uniformly approximated by a function $g \in A$ with arbitrary accuracy (Levin et al., 2013; Fermanian, 2021).

From the above reasoning, we can construct a nonlinear predictor as a linear combination of iterated integrals for each segment of the multidimensional time series.

2.2. Procedure for machine learning of time series

In the proposed approach, the predictor is constructed as follows. Suppose we have a time series of several climate indices defined at each calendar month of t_m , $m = 1, 2, \dots, M$. Any segment of the time series over a period, say six months, can be viewed as a multidimensional path, which can be represented by the signature.

For this supervised learning, the object variable is the NINO3.4 index y_{m+m_a} at time $\tau = t_{m+m_a}$, while the explanatory variables x_m are the signature for the segment of time series X in the period $[t_{m-m_b+1}, t_m]$. The approximation property described in the previous section allows us to express the object variable as a linear combination of the explanatory variables:

$$y_{m+m_a} = y_m + \langle w_m, x_m \rangle + \epsilon, \quad (5)$$

$$x_m := S_n(X_{[t_{m-m_b+1}, t_m]}), \quad (6)$$

where $S_n(X_{[t_0, t_1]})$ denotes the order- n signature for the d -dimensional time series in the interval $[t_0, t_1]$, $\langle a, b \rangle$ denotes the scalar product $\sum_I a^{(I)} b^{(I)}$, $w_m = \{w_m^{(I)} | I = \text{multi-index}\}$ is the weight vector for the predictor, ϵ is a random variable representing prediction error, t_m is the starting time of the prediction, t_{m-m_b+1} is the starting point of the path segment, and t_{m+m_a} is the target time for prediction. Before converting into the signature, a zero vector is added at the beginning of each series $X_{[t_{m-m_b+1}, t_m]}$ to account for the magnitude of the value at the starting point (Morrill et al., 2021). We computed the signature by using the Python library `esig` (Kormilitzin, 2017).

In the control case, we instead used the time series as is without converting it into the signature:

$$x_m := X_{[t_{m-m_b+1}, t_m]} = (X_{t_{m-m_b+1}}, X_{t_{m-m_b+2}}, \dots, X_{t_m}). \quad (7)$$

This corresponds to an auto-regressive (AR) model.

Using the training dataset available up to time t_m ,

$$D_m = \left\{ \left(x_\mu, y_{\mu+m_a} - y_\mu \right) \mid \mu \in [m_b, m - m_a] \right\}, \quad (8)$$

we first estimate the optimal weight $w = w_m$ that minimizes the cost function with an L_1 -penalty term:

$$J_m(w) = \frac{1}{2|D_m|} \sum_{\mu=m_b}^{m-m_a} \left(y_{\mu+m_a} - y_\mu - \langle w, x_\mu \rangle \right)^2 + \alpha \sum_I |w^{(I)}|, \quad (9)$$

where $|D_m| = m - m_a - m_b + 1$ is the number of samples in D_m , and I is the multi-index. The optimization problem is solved by the Lasso model fit with least angle regression (Pedregosa et al., 2011), which is suitable for problems with

many parameters. We then predict a future NINO3.4 index as $\hat{y}_{m+m_a} = y_m + \langle w_m, x_m \rangle$ and compare it to y_{m+m_a} . In other words, a cross-validation is made against the validation data:

$$D'_m = \left\{ \left(x_m, y_{m+m_a} - y_m \right) \right\}. \quad (10)$$

We repeat the above procedure after incrementing the time index m by 1.

Figure 1 shows the schematic view of training and prediction flow. In this flow, the weight w_m is obtained by using the training dataset D_m , and then the prediction from time t_m using the signature x_m yields the value \hat{y}_{m+m_a} , which is subject to comparison with the validation data y_{m+m_a} . Note that the size of the training data $|D_m| = m - m_a - m_b + 1$ depends on the starting time t_m . The prediction error can be obtained from the statistics of $\hat{y}_{m+m_a} - y_{m+m_a}$ for various starting times. By taking this approach, where training and forecasts are done progressively by moving the starting time of the forecast hiding future at that moment, each forecast is assured to be a fair cross-validation.

2.3. Diagnosing the dominant event sequences

One difficulty with regular machine learning is that it does not provide sufficient reasoning for the results. However, the signature-based method allows us to mathematically extract from the path those properties that are important in the prediction.

To diagnose the dominant event sequences that contribute to the prediction, we compute the standard partial regression coefficients (SPRCs) $r_m^{(I)}$, which represent the sensitivity of normalized value $y_{\mu+m_a}$ in the future to each component of the normalized signature $x_\mu^{(I)}$ in the past, as

$$r_m^{(I)} = \frac{\sigma_{x_m^{(I)}}}{\sigma_{y_m}} w_m^{(I)}, \quad (11)$$

where σ_{y_m} and $\sigma_{x_m^{(I)}}$ denote the standard deviations of $y_{\mu+m_a} - y_\mu$ and $x_\mu^{(I)}$, respectively, among the samples in D_m , which represents the learning data in the period from time t_{m_b} to time t_{m-m_a} .

2.4. Setting of experimental parameters

We used a climate time series composed of $d = 12$ indices in Table 1 retrieved from NOAA cite (NOAA, 2021). The time series starts at t_1 (January of 1900), and ends at t_{1459} (July of 2021).

The standard lead time for prediction is 6 months ($m_a = 6$), whereas each past segment is of length 6 months ($m_b = 6$). The experiment duration was from the prediction starting at t_{961} (January of 1980), to the one starting at t_{1453} (January of 2021).

We used iterated integrals up to level $n = 3$, which means that the total number of terms in the linear combination

Table 1

Twelve climate indices and their abbreviations

| Abbrev. | Climate Indices | References |
|---------|--|------------------------------|
| NINO34 | Nino 3.4 (5N-5S, 170W-120W) SST | Rayner et al. (2003) |
| NINO12 | Nino 1+2 (0-10S, 90W-80W) SST | Rayner et al. (2003) |
| NINO3 | Nino 3 (5N-5S, 150W-90W) SST | Rayner et al. (2003) |
| NINO4 | Nino 4 (5N-5S, 160E-150W) SST | Rayner et al. (2003) |
| DMI | Dipole Mode Index | Hameed and Yamagata (2003) |
| AMO | Atlantic Multidecadal Oscillation index | Enfield et al. (2001) |
| NPI | North Pacific Index | Trenberth and Hurrell (1994) |
| SOI | Southern Oscillation Index | Ropelewski and Jones (1987) |
| NAO | North Atlantic Oscillation (NAO) index | Jones et al. (1997) |
| TPI | Tripole Index | Henley et al. (2015) |
| AO | Arctic Oscillation index | Thompson and Wallace (1998) |
| MON | Date elapsed (mid-day in month divided by 365) | - |

was $N = (d^{n+1} - 1)/(d - 1) = 1885$, and the intensity of the L_1 penalty term was tuned to $\alpha = 2.0$.

3. Results

Figure 2 shows the result of 6-month prediction, whereas fig 3 shows it as anomalies from climatology, These figures indicate the overall superiority of prediction using the signature. The prediction error for each target month is shown in Fig. 4. It is obvious that the predictions for July to September were much better than those in the control case; however, they were comparable in the other months. The overall prediction skill was 0.596K for the signature case and 0.663K for the control case.

Wang et al. (2020) proposed an operator-theoretic technique called kernel analog forecasting (KAF), which has a rigorous connection with Koopman operator theory for dynamical systems, yielding statistically optimal predictions as conditional expectations. They also compared it to the linear inverse model (LIM), which is a linear evolution operator for modes. Note that both methods employ as explanatory variables the dominant modes in spatiotemporal SST, which we did not use in our study. Here, we use KAF and LIM for the comparison of forecasting skill. For the comparison with KAF and LIM, the root-mean square (rms) errors for 6-month prediction in the period from 1998 to 2017 were computed. The signature model, AR model, KAF model, and LIM had rms values of 0.617, 0.686, 0.62, and 0.75K, respectively. This comparison result suggests that the forecasting skill of the signature model is comparable to that of the KAF model.

The spring prediction barrier is defined in Lai et al. (2018) as follows: "... models have problems in predicting Boreal winter tropical Pacific sea surface temperature (SST) when forecasts start in Boreal spring (February–May). This is called the spring predictability barrier." Similarly, Zheng and Zhu (2010) pointed out that "... errors have the largest values and the fastest growth rates initialized before and during the NH spring." In light of these definitions, the spring predictability barrier, i.e., poor prediction skill when starting from February and March, seems to disappear

Table 2

Top five dominant event sequences among iterated integrals. "1st" denotes the first index for the corresponding iterated integral: $S^{(i_1 i_2 i_3)}(X) = \int_s^t \int_s^{t_3} \int_s^{t_2} dX_{t_1}^{(i_1)} dX_{t_2}^{(i_2)} dX_{t_3}^{(i_3)}$. Events happen from first to third: $t_1 < t_2 < t_3$. If the same index appears twice in a row, then the event is intense. "SPRC" represents the standard partial regression coefficients (Eq. 11).

| Learning data from Jan. 1900 to Dec. 1999 | | | | |
|---|-------------------------------|-------------------------------|---------------|---------------|
| No. | SPRC $r_m^{(i_1 i_2 i_3)}$ | Indices in iterated integrals | | |
| | | 1st (i_1) | 2nd (i_2) | 3rd (i_3) |
| 1 | 5.55 | NPI | NINO3 | NPI |
| 2 | -3.70 | NINO3 | NPI | NPI |
| 3 | 3.63 | NPI | NPI | NINO12 |
| 4 | -3.57 | NINO34 | NINO34 | NINO34 |
| 5 | 3.34 | NINO34 | NPI | NPI |
| Learning data from Jan. 1900 to Dec. 2020 | | | | |
| No. | SPRC $r_m^{(i_1 i_2 i_3)}$ | Indices in iterated integrals | | |
| | | 1st (i_1) | 2nd (i_2) | 3rd (i_3) |
| 1 | 4.53 | NPI | NPI | NINO12 |
| 2 | -4.17 | NINO34 | NINO34 | NPI |
| 3 | -3.37 | NPI | NINO34 | NINO12 |
| 4 | -3.25 | NINO34 | NPI | NINO12 |
| 5 | 2.88 | NPI | NINO3 | NPI |

as indicated by the rms error values in the target months of August to September.

Table 2 shows the dominant event sequences among iterated integrals. The events with the first to the third indices are shown in each row. If the same index appears twice in a row, then the event is intense. The top sequence in the period from 1900 to 2020 is an intense NPI change followed by a Niño 1+2 SST change. The key indices are NPI and various NINO indices. In particular, NPI, an atmospheric process, is involved in all the dominant sequences, which should be a manifestation that El Niño is a coupled atmospheric–oceanic process. In addition, the comparison between statistics for two different periods suggests that the Niño1+2 index, corresponding to the region of coastal South America, is becoming more important as a precursor in the 21st century. Summarizing the above, fig. 5 illustrates how the dominant climate events occur that will lead to changes in the future NINO3.4.

Although the main indices in terms of the iterative integrals are related to water temperature in the NINO regions, it appears that not only these but also various climate indices contribute incrementally, and the predictor is built on the balance of them. In fact, if we perform an experiment with the main 5 indices (NINO12, NINO3, NINO34, NINO4, and NPI), the rms error for the prediction is 0.666K, with no improvement from the control case. In this respect, the inference structure is considered to be different from other SST-based predictions such as KAF and LIM.

4. Conclusions

We developed a model that can statistically predict El Niño using only the time series of past multidimensional climate indices. By converting the time series into the signature, the accuracy of the machine learning algorithm is improved and, thereby, the NINO3.4 SST can be predicted to some extent six months in advance. An important byproduct

of this approach is that the correlation of climate events can be read from the dominant iterative integral. For example, it was suggested that variations in the NPI, NINO12, and other indices occur in a certain order, which leads to variations in the NINO3.4 SST. It was also found that the signature method can learn the nonlinear development of El Niño more accurately than the traditional AR model and, thus, is less sensitive to the spring barrier of predictability. Future research is required to improve the scheme by incorporating more detailed oceanographic information, evaluating uncertainties, and considering other factors.

The predictions obtained by this method are not marked with error bars, but because we know the prediction error for each month as shown in Fig. 4, we can consider these values as the prediction error. However, as it is not possible to give a forecast error for each forecast individually, an ensemble could be created by bootstrapping or other methods to improve this point, which may also lead to a factory for forecast accuracy.

The length of the path segment used for the 6-month forecast, 6 months, was confirmed in preliminary experiments (not shown) to be appropriate, but the length of the path segment required for forecasts with other lead times may be different. It is also necessary to confirm whether the step-3 signature is optimal.

The dominant iterated integral for prediction may change from time to time depending on the period covered, as shown in Table 2. It needs to be carefully considered how this relates to the decadal changes in the Niño mechanism. These points remain as future work.

5. Acknowledgments

This study was funded by JST-PROJECT-20218919.

Code availability section

Name: enso_signature

Contact: nsugiura@jamstec.go.jp, +81-46-867-9054

Hardware requirements: CPU

Program language: Python

Software required: Python libraries esig and scikit-learn

Program size: 188 lines

The source codes are available for downloading at the link: https://github.com/nozomi-sugiura/enso_signature

References

- Alexander, M.A., Bladé, I., Newman, M., Lanzante, J.R., Lau, N.C., Scott, J.D., 2002. The atmospheric bridge: The influence of ENSO teleconnections on air–sea interaction over the global oceans. *Journal of climate* 15, 2205–2231.
- Bjerknes, J., 1969. Atmospheric teleconnections from the equatorial Pacific. *Monthly weather review* 97, 163–172.
- Dijkstra, H.A., Petersik, P., Hernández-García, E., López, C., 2019. The application of machine learning techniques to improve El Niño prediction skill. *Frontiers in Physics* 7, 153.
- Enfield, D.B., Mestas-Nuñez, A.M., Trimble, P.J., 2001. The atlantic multidecadal oscillation and its relation to rainfall and river flows in the continental u.s. *Geophysical Research Letters* 28, 2077–2080. URL: <https://agupubs.onlinelibrary.wiley.com/doi/abs/10.1029/2000GL012745>, doi:<https://doi.org/10.1029/2000GL012745>, arXiv:<https://agupubs.onlinelibrary.wiley.com/doi/pdf/10.1029/2000GL012745>.
- Fermanian, A., 2021. Embedding and learning with signatures. *Computational Statistics & Data Analysis* 157, 107148.
- Ham, Y.G., Kim, J.H., Luo, J.J., 2019. Deep learning for multi-year enso forecasts. *Nature* 573, 568–572. doi:<https://doi.org/10.1038/s41586-019-1559-7>.
- Hameed, S., Yamagata, T., 2003. Possible impacts of indian ocean dipole mode events on global climate. *Climate Research - CLIMATE RES* 25, 151–169. doi:10.3354/cr025151.
- Henley, B.J., Gergis, J., Karoly, D.J., Power, S., Kennedy, J., Folland, C.K., 2015. A Tripole Index for the Interdecadal Pacific Oscillation. *Climate Dynamics* 45, 3077–3090. doi:10.1007/s00382-015-2525-1.
- Hu, X., Eichner, J., Faust, E., Kantz, H., 2021. Benchmarking prediction skill in binary el niño forecasts. *Climate Dynamics* , 1–15.
- Jones, P.D., Jonsson, T., Wheeler, D., 1997. Extension to the north atlantic oscillation using early instrumental pressure observations from gibraltar and south-west iceland. *International Journal of Climatology* 17, 1433–1450. doi:[https://doi.org/10.1002/\(SICI\)1097-0088\(19971115\)17:13<1433::AID-JOC203>3.0.CO;2-P](https://doi.org/10.1002/(SICI)1097-0088(19971115)17:13<1433::AID-JOC203>3.0.CO;2-P).
- Kormilitzin, A., 2017. the-signature-method-in-machine-learning. <https://github.com/kormilitzin/>.
- Lai, A.W.C., Herzog, M., Graf, H.F., 2018. Enso forecasts near the spring predictability barrier and possible reasons for the recently reduced predictability. *Journal of Climate* 31, 815–838.
- Levin, D., Lyons, T., Ni, H., 2013. Learning from the past, predicting the statistics for the future, learning an evolving system. ArXiv e-prints arXiv:1309.0260.
- Lyons, T.J., Caruana, M., Lévy, T., 2007. Differential Equations Driven by Rough Paths. volume 1908 of *Lecture Notes in Mathematics*. Springer.

- Morrill, J., Fermanian, A., Kidger, P., Lyons, T., 2021. A Generalised Signature Method for Multivariate Time Series Feature Extraction. *arXiv:2006.00873*.
- Nakamura, T., Tachibana, Y., Honda, M., Yamane, S., 2006. Influence of the Northern Hemisphere annular mode on ENSO by modulating westerly wind bursts. *Geophysical Research Letters* 33.
- Neelin, J.D., Battisti, D.S., Hirst, A.C., Jin, F.F., Wakata, Y., Yamagata, T., Zebiak, S.E., 1998. Enso theory. *J. Geophys. Res.* 103, 14 261–14 290.
- NOAA, 2021. Climate Timeseries at PSL. URL: https://psl.noaa.gov/gcos_wgsp/Timeseries/.
- Pedregosa, F., Varoquaux, G., Gramfort, A., Michel, V., Thirion, B., Grisel, O., Blondel, M., Prettenhofer, P., Weiss, R., Dubourg, V., Vanderplas, J., Passos, A., Cournapeau, D., Brucher, M., Perrot, M., Duchesnay, E., 2011. Scikit-learn: Machine learning in Python. *Journal of Machine Learning Research* 12, 2825–2830.
- Penland, C., Magorian, T., 1993. Prediction of Niño 3 Sea Surface Temperatures Using Linear Inverse Modeling. *Journal of Climate* 6, 1067 – 1076. URL: https://journals.ametsoc.org/view/journals/clim/6/6/1520-0442_1993_006_1067_ponsst_2_0_co_2.xml, doi:10.1175/1520-0442(1993)006<1067:PONSST>2.0.CO;2.
- Rayner, N.A., Parker, D.E., Horton, E.B., Folland, C.K., Alexander, L.V., Rowell, D.P., Kent, E.C., Kaplan, A., 2003. Global analyses of sea surface temperature, sea ice, and night marine air temperature since the late nineteenth century. *Journal of Geophysical Research: Atmospheres* 108. URL: <https://agupubs.onlinelibrary.wiley.com/doi/abs/10.1029/2002JD002670>, doi:<https://doi.org/10.1029/2002JD002670>, arXiv:<https://agupubs.onlinelibrary.wiley.com/doi/pdf/10.1029/2002JD002670>.
- Ropelewski, C.F., Jones, P.D., 1987. An extension of the tahiti–darwin southern oscillation index. *Monthly weather review* 115, 2161–2165.
- Stone, M., 1937. Applications of the theory of boolean rings to general topology. *Transactions of the American Mathematical Society* 41, 375–481.
- Sugiura, N., Hosoda, S., 2020. Machine learning technique using the signature method for automated quality control of argo profiles. *Earth and Space Science* 7, e2019EA001019. URL: <https://agupubs.onlinelibrary.wiley.com/doi/abs/10.1029/2019EA001019>, doi:<https://doi.org/10.1029/2019EA001019>, arXiv:<https://agupubs.onlinelibrary.wiley.com/doi/pdf/10.1029/2019EA001019>, e2019EA001019 10.1029/2019EA001019.
- Thompson, D.W.J., Wallace, J.M., 1998. The arctic oscillation signature in the wintertime geopotential height and temperature fields. *Geophysical Research Letters* 25, 1297–1300. URL: <https://agupubs.onlinelibrary.wiley.com/doi/abs/10.1029/98GL00950>, doi:<https://doi.org/10.1029/98GL00950>, arXiv:<https://agupubs.onlinelibrary.wiley.com/doi/pdf/10.1029/98GL00950>.
- Timmermann, A., An, S.I., Kug, J.S., Jin, F.F., Cai, W., Capotondi, A., Cobb, K.M., Lengaigne, M., McPhaden, M.J., Stuecker, M.F., et al., 2018. El niño–southern oscillation complexity. *Nature* 559, 535–545.
- Trenberth, K., Hurrell, J., 1994. Decadal atmosphere-ocean variations in the Pacific. *Climate Dynamics* 9, 303–319. doi:<https://doi.org/10.1007/BF00204745>.
- Vimont, D.J., Wallace, J.M., Battisti, D.S., 2003. The seasonal footprinting mechanism in the Pacific: Implications for ENSO. *Journal of Climate* 16, 2668–2675.
- Wallace, J.M., Rasmusson, E.M., Mitchell, T.P., Kousky, V.E., Sarachik, E.S., von Storch, H., 1998. On the structure and evolution of enso related climate variability in the tropical pacific: Lessons from toga. *J. Geophys. Res.* 103, 14 241–14 259.
- Wang, X., Slawinska, J., Giannakis, D., 2020. Extended-range statistical ENSO prediction through operator-theoretic techniques for nonlinear dynamics. *Sci Rep.* 10, 2636. doi:10.1038/s41598-020-59128-7.
- White, C.J., Hudson, D., Alves, O., 2014. ENSO, the IOD and the intraseasonal prediction of heat extremes across Australia using POAMA-2. *Climate dynamics* 43, 1791–1810.

Simple El Niño prediction

- Wu, X., Okumura, Y.M., Deser, C., DiNezio, P.N., 2021. Two-Year Dynamical Predictions of ENSO Event Duration during 1954–2015. *Journal of Climate* 34, 4069 – 4087. URL: <https://journals.ametsoc.org/view/journals/clim/34/10/JCLI-D-20-0619.1.xml>, doi:10.1175/JCLI-D-20-0619.1.
- Yan, J., Mu, L., Wang, L., Ranjan, R., Zomaya, A.Y., 2020. Temporal convolutional networks for the advance prediction of ENSO. *Scientific reports* 10, 1–15.
- Zheng, F., Zhu, J., 2010. Spring predictability barrier of ENSO events from the perspective of an ensemble prediction system. *Global and Planetary Change* 72, 108–117.

List of Figures

| | | |
|---|---|----|
| 1 | Schematic view of training and prediction flow, assuming that $m_b=m_a=6$. Hatched squares represent transforming into the signature. Predicted value at time index $m+6$ will be compared with the validation data if available. | 13 |
| 2 | Comparison of NINO3.4 for 6-month predictions. Red: signature case; blue: control case. Horizontal axis is the target year and month, and vertical axis is temperature in °C. | 14 |
| 3 | The same as Fig. 2 but shown as anomalies, which are defined as the difference from the past 30-yr mean of monthly values. Red: signature case; blue: control case. Horizontal axis is the target year and month, and vertical axis is temperature anomalies in °C. | 15 |
| 4 | Prediction error for each target month. Red: signature case; blue: control case. Horizontal axis is the target month (1 = January, 2 = February, ..., 12 = December), and vertical axis is rms error in K. | 15 |
| 5 | Typical climate event flows for predicting future Nino3.4 index. Arrows indicate time order. Key indices include NINO12 (Nino1+2 SST), NINO34 (Nino3.4 SST), NINO4 (Nino4 SST), and NPI (North Pacific Index). | 16 |

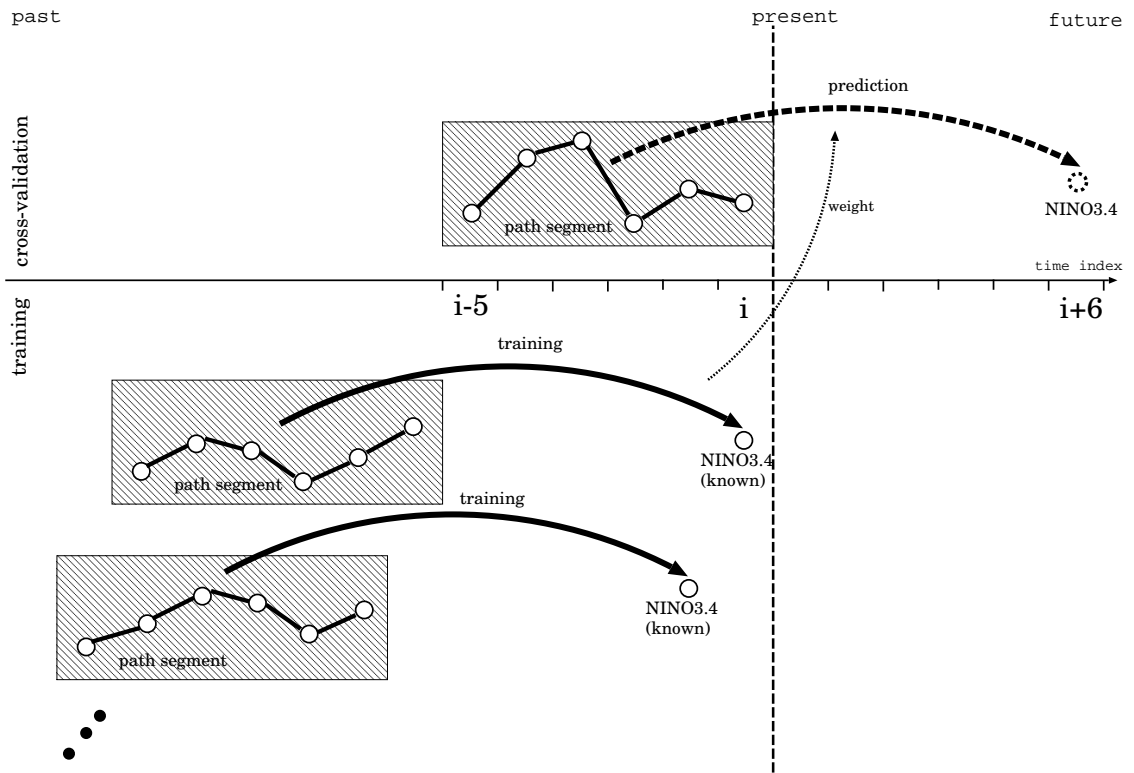


Figure 1: Schematic view of training and prediction flow, assuming that $m_b=m_a=6$. Hatched squares represent transforming into the signature. Predicted value at time index $m+6$ will be compared with the validation data if available.

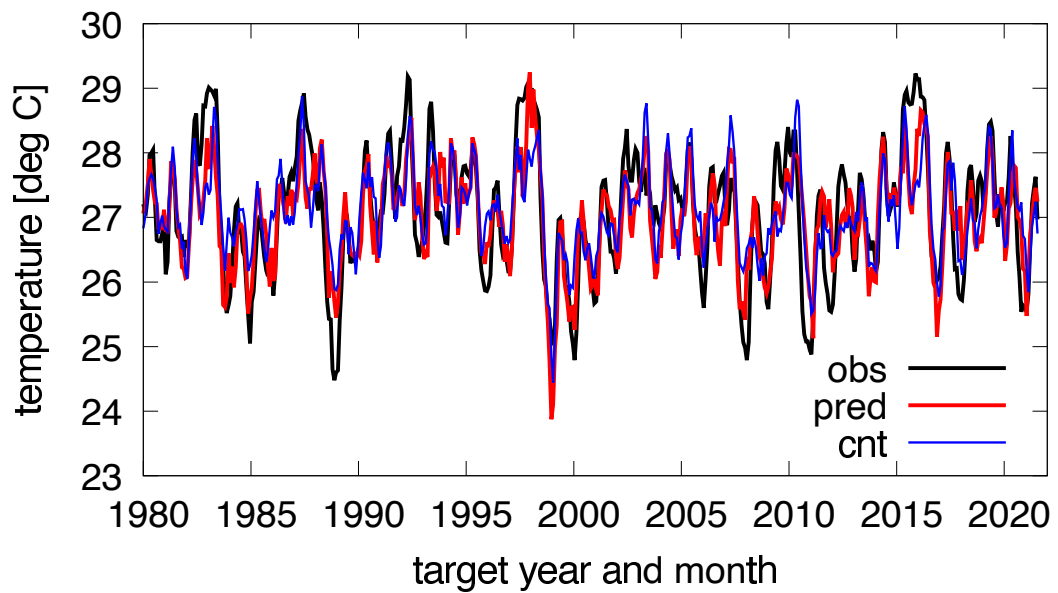


Figure 2: Comparison of NINO3.4 for 6-month predictions. Red: signature case; blue: control case. Horizontal axis is the target year and month, and vertical axis is temperature in °C.

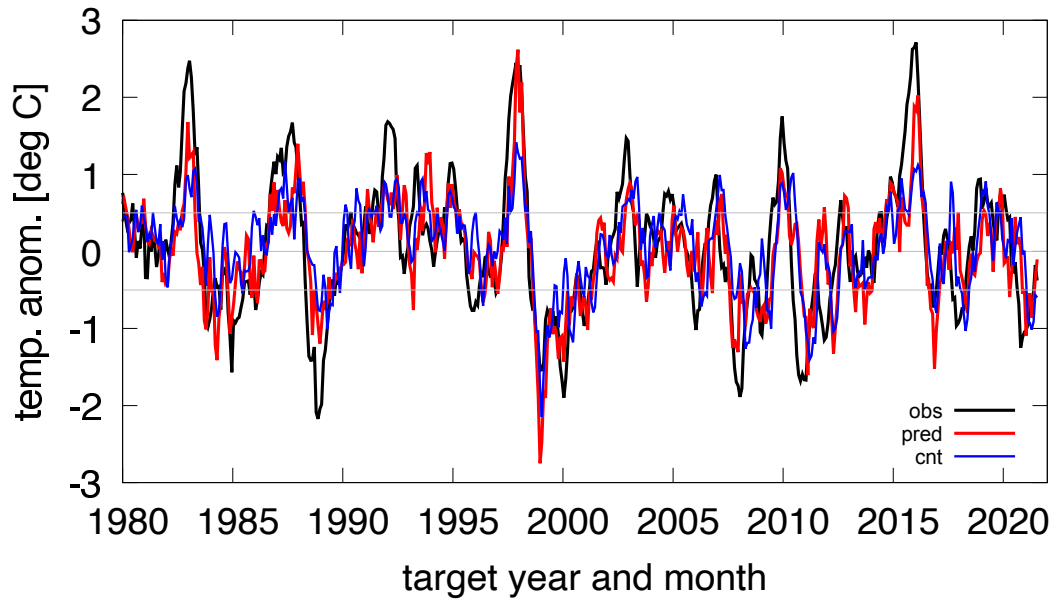


Figure 3: The same as Fig. 2 but shown as anomalies, which are defined as the difference from the past 30-yr mean of monthly values. Red: signature case; blue: control case. Horizontal axis is the target year and month, and vertical axis is temperature anomalies in °C.

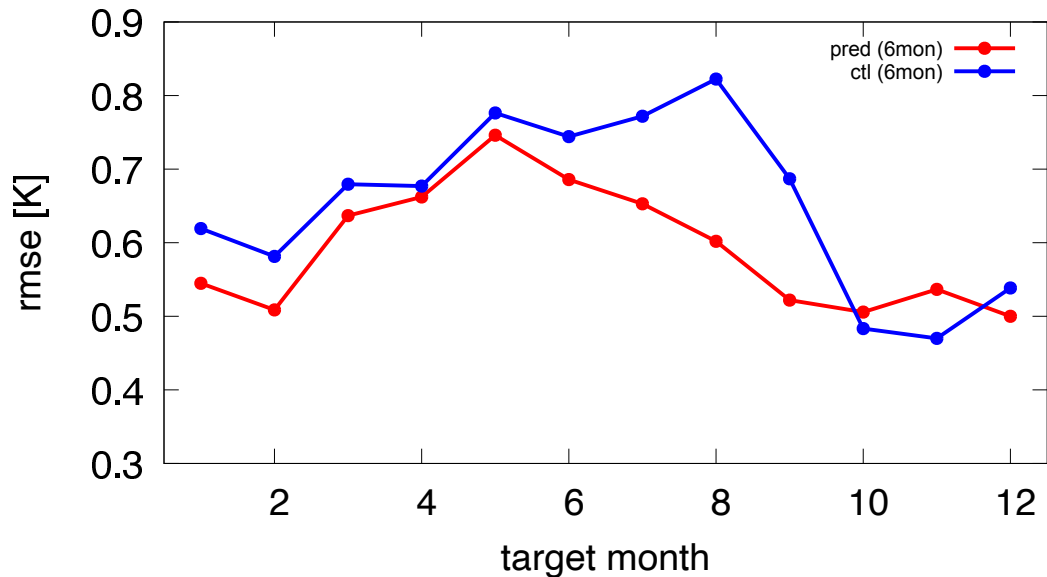


Figure 4: Prediction error for each target month. Red: signature case; blue: control case. Horizontal axis is the target month (1 = January, 2 = February, ..., 12 = December), and vertical axis is rms error in K.

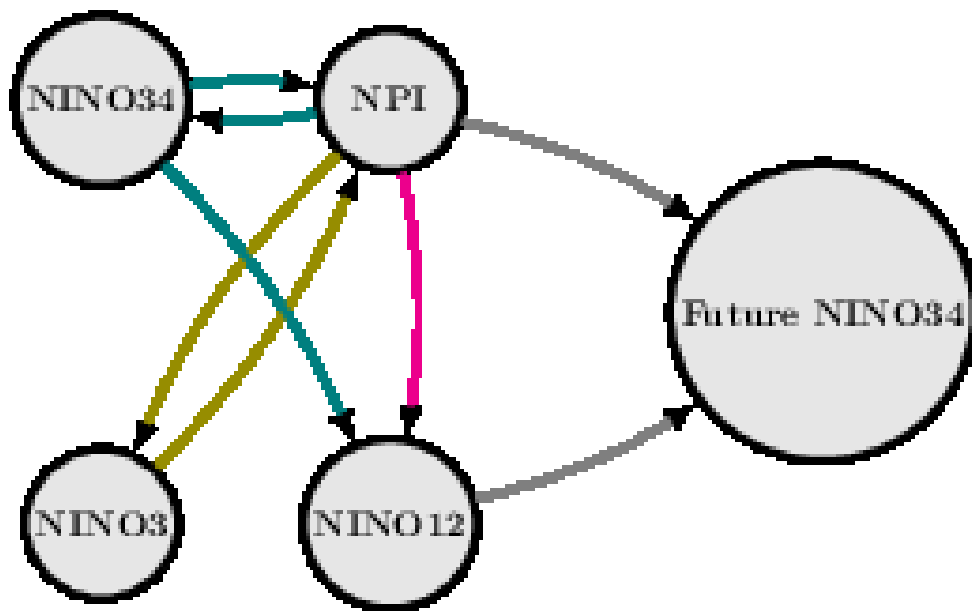


Figure 5: Typical climate event flows for predicting future Nino3.4 index. Arrows indicate time order. Key indices include NINO12 (Nino1+2 SST), NINO34 (Nino3.4 SST), NINO4 (Nino4 SST), and NPI (North Pacific Index).